Diffusion on curved, periodic surfaces

R. Hołyst, D. Plewczyński, and A. Aksimentiev
Department III, Institute of Physical Chemistry, PAS and College of Science, Kasprzaka 44/52, 01-224 Warsaw, Poland

K. Burdzy
Department of Mathematics, University of Washington, Seattle, Washington 98195

(Received 26 January 1999)

We present a simulation algorithm for a diffusion on a curved surface given by the equation $\phi(\mathbf{r})=0$. The algorithm is tested against analytical results known for diffusion on a cylinder and a sphere, and applied to the diffusion on the *P*, *D*, and *G* periodic nodal surfaces. It should find application in an interpretation of two-dimensional exchange NMR spectroscopy data of diffusion on biological membranes. [S1063-651X(99)12107-X]

PACS number(s): 05.40.−a, 87.64.Hd, 87.16.−b

I. INTRODUCTION

Transport modes of molecules in a living cell, i.e., in a cytoplasm [1], between the cytoplasm and the nucleus [2,3], or along biological membranes [4], should provide direct information about the architecture of living cells on microscopic and mesoscopic levels. So far, studies focused on the discrimination between directional and diffusional motion in living organisms [4] and the sole quantity determined from them was the diffusion constant [1–4]. New experimental NMR techniques combined with new theoretical tools are expected to yield information about the geometry and topology of the region where the diffusion takes place [5]. In the spirit of Kac's famous question, ''Can one hear the shape of a drum?'' [6] or, in other words, can we obtain the geometry of the region from the spectrum of the diffusion operator in that region?

The method of two-dimensional exchange spectroscopy in ^{2}H NMR, originally developed by Wefing and Spiess [7] to study the slow reorientation of molecules in solids, has been recently applied to diffusion on lipid membranes on microscopic and mesoscopic scales [8–11]. The typical length scale probed by the technique ranges from tens of Å up to tens of thousands of Å, and the typical times range from tens of microseconds up to hundreds of milliseconds or even seconds. This experimental technique provides a direct quantitative measure of the space-time correlation function of the orientation of local surface normals for individual molecules [8–11]. A molecule diffusing on a lipid membrane changes its orientation in time because of the curvature of the membrane, and from NMR experiments in the case of an axially symmetric coupling tensor one obtains the probability $P(\beta,t)$, that in time t the orientation $\mathbf{n}$ changes by the angle β [8–11],

$$\cos\beta=\mathbf{n}(0)\cdot\mathbf{n}(t). \tag{1}$$

The probability $P(\beta,t)$ is called the reorientational angle distribution (RAD). Due to the symmetry properties one in fact probes the symmetrized function $P_{\mathrm{sym}}(\beta,t)=P(\beta,t)+P(\pi-\beta,t)$. From this correlation function some geometrical and topological properties such as Gaussian and mean curvatures and the distribution of orientations of the vectors normal to the membrane can be extracted. The interpretation of the experimental data is hampered by the lack of theoretical tools. In particular there is no simple and general algorithm in physics for solving the diffusion problem on a curved surface given by the general equation

$$\phi(\mathbf{r})=0. \tag{2}$$

The diffusion equation can be explicitly solved only in some special cases (e.g., a sphere or a cylinder) but not in the general case of Eq. (2). In this paper we present a general simulation algorithm for studying diffusion on any surface given by Eq. (2), and apply it to the diffusion on periodic, nodal surfaces introduced by Mackay [12]. It has been shown recently that inner membranes (endoplasmatic reticulum) inside living cells form periodic surfaces [13], and that is why we have decided to apply the method first to periodic surfaces.

The paper is organized as follows. In Sec. II we present an algorithm for diffusion on a curved surface given by Eq. (2). In Sec. III we compare numerical results with the analytical solutions for a cylinder and a sphere. In Sec. IV we discuss the stability of the algorithm for diffusion on the *P* periodic surface. Here we also discuss the diffusion on *D* and *G* periodic surfaces. A summary is contained in Sec. V.

II. SIMULATION METHOD

We consider the diffusion of a particle on a surface given by Eq. (2). The diffusion will be represented as a random walk. The simulation algorithm consists of the following steps. A particle starts at point $\mathbf{r}_0$ on the surface. A plane tangent at $\mathbf{r}_0$ to the surface is given by the equation

$$(\mathbf{r}-\mathbf{r}_0)\cdot\nabla\phi(\mathbf{r}_0)=0, \tag{3}$$

where the nabla operator acting on a scalar function $\phi(\mathbf{r})$ is taken at point $\mathbf{r}_0$. In the tangent plane we randomly choose a direction from 0 to 2π. Next the particle jumps along this direction up to a point $\mathbf{r}_1$. The length of the jump, $L=|\mathbf{r}_1-\mathbf{r}_0|$, is drawn from the distribution

$$\varrho(L)=\frac{L}{2D_0\tau_0}\exp\left(-\frac{L^2}{4D_0\tau_0}\right), \tag{4}$$

where D_0 is a local diffusion coefficient, and τ_0 is the duration of the time step. Our normalization of D_0 is such that the typical size of a jump is equal to $\sqrt{4D_0\tau_0}$. Next we project the point $\mathbf{r}_1$ onto the surface along the direction given by $\nabla\phi(\mathbf{r}_1)$. The final location on the surface, $\mathbf{r}_2$, after one simulation step, is therefore

$$\mathbf{r}_2=\mathbf{r}_1-\frac{\phi(\mathbf{r}_1)\nabla\phi(\mathbf{r}_1)}{|\nabla\phi(\mathbf{r}_1)|^2}. \tag{5}$$

This follows from the fact that $\nabla\phi(\mathbf{r}_1)\approx\nabla\phi(\mathbf{r}_2)$, $\phi(\mathbf{r}_2)=0$, and the expansion of $\phi(\mathbf{r}_2)$ in $(\mathbf{r}_2-\mathbf{r}_1)$. Note that in the limit of $L\to 0$ we have

$$|\mathbf{r}_2-\mathbf{r}_1|\sim L^2. \tag{6}$$

The step is next repeated from the new starting point given by Eq. (5).

The algorithm is stable and satisfies the detailed balance condition, providing that the steps are much smaller than the typical radius of curvature of the surface. The detailed balance condition is given by $T(A|B)P(B)=T(B|A)P(A)$, where $T(B|A)$ is the transition probability from A to B, and $P(A)$ is the probability of being at point A. In the stationary state the probability for a Brownian particle being at any point on the surface is constant, i.e., $P(A)=P(B)$ for any A and B. Therefore one should prove that $T(A|B)=T(B|A)$. In our case it is sufficient to prove that if we start the procedure at $\mathbf{r}_2$ then we will finish at $\mathbf{r}_0$ with the same probability as that for the transition from $\mathbf{r}_0$ to $\mathbf{r}_2$. The steps of the algorithm generate a path $\mathbf{r}_0\to\mathbf{r}_1\to\mathbf{r}_2$. Now we repeat the algorithm backwards starting at $\mathbf{r}_2$, and we find $\mathbf{r}_2\to\mathbf{r}_1^*\to\mathbf{r}_0^*$. The jump length has the same distribution in both cases, and so we might randomly generate $\mathbf{r}_1^*$ in such a way that $|\mathbf{r}_2-\mathbf{r}_1^*|=|\mathbf{r}_1-\mathbf{r}_0|=L$ (this is assumed only for the sake of argument; the true algorithm steps are independent). A similar argument applies to the jump direction. Now it is sufficient to show that $|\mathbf{r}_0-\mathbf{r}_0^*|$ is much smaller than the jump length L. Following the discussion after Eqs. (5) and (6), it is not hard to see that in the limit of $L\to 0$ we have

$$|\mathbf{r}_0-\mathbf{r}_0^*|\sim L^2, \tag{7}$$

which proves the detailed balance condition. The algorithm breaks down when L is comparable to the local radius of curvature, as shown in Sec. IV.

III. METHOD TESTGROUND OF THE SIMULATION

The numerical details of our algorithm are as follows. First we take any point at the surface and start the random walk from this point. Since in the long time limit a single random walker will visit all the points on the surface many times, the exact location of the starting point is not important. The typical run consists of $M=10^8$ time steps, each of duration τ_0. The typical length of each step is $J=1.0\sqrt{4D_0\tau_0}$ (see Sec. II), in comparison to the typical linear size of studied structures equal to $\sim 100.0\sqrt{4D_0\tau_0}$.

The averages at time $t=N\tau_0$ are taken over $m=M/N$ points. For example, the average of the cosine of the reorientational angle β [Eq. (1)] at time t is

$$\langle\cos\beta(t)\rangle=\sum_{i=1}^{m}\frac{\mathbf{n}(t_i-t)\cdot\mathbf{n}(t_i)}{m}, \tag{8}$$

where $\mathbf{n}(t_i)$ is the unit vector normal to the surface at the point reached by the random walker at time $t_i=iN\tau_0$. For our purpose $m=M/N$ points are sufficient for calculations of the averages, but, in general, in order to improve statistics, one can use every point on this single path of length M. The maximum number of points that can be used for the calculation of the averages at time $t=N\tau_0$ is $M-N$, and the final formula for the average of the cosine of the reorientational angle β at time t is

$$\langle\cos\beta(t)\rangle=\sum_{i=1}^{m-1}\sum_{j=1}^{N}\frac{\mathbf{n}(t_i-t+j\tau_0)\cdot\mathbf{n}(t_i+j\tau_0)}{M-N}. \tag{9}$$

This procedure for a very long single trajectory is equivalent to the calculation of averages for $M-N$ trajectories of length N starting at randomly chosen points at the surface with a uniform distribution (see also the discussion of the detailed balance condition). In this case the average is

$$\langle\cos\beta(t)\rangle=\sum_{i=1}^{M-N}\frac{\mathbf{n}_i(t)\cdot\mathbf{n}_i(0)}{M-N}, \tag{10}$$

where the index i corresponds to the ith trajectory. This equivalence is due to the ergodicity and the Markov nature of the random walk.

We have tested the algorithm against analytical results known for a sphere and a cylinder. For numerical simulations we take a sphere of radius $R=43.0\sqrt{4D_0\tau_0}$ and a cylinder of radius $r=43.0\sqrt{4D_0\tau_0}$. The RAD for a sphere of radius R, following from the solution of the diffusion equation, has the form:

$$P_S(\beta,t)=\tfrac{1}{2}\sum_{l=0}^{\infty}(2l+1)P_l(\cos\beta)\times\exp\left(-t\frac{l(l+1)D_0}{R^2}\right)\sin\beta, \tag{11}$$

where P_l are the Legendre polynomials and β is the polar angle in this case. The RAD for a cylinder of radius R is

$$P_C(\beta,t)=\frac{1}{2\pi}\left[1+2\sum_{n=1}^{\infty}\cos(n\beta)\exp\left(-t\frac{D_0n^2}{R^2}\right)\right]. \tag{12}$$

The comparison with the simulations is illustrated in Figs. 1 and 2. We start with a distribution strongly peaked at $\beta=0$. Then in the course of the evolution the distribution spreads, and in a time proportional to R^2 reaches the stationary distribution. The latter quantity is the orientational distribution of the vectors normal to the surface. In the case of a sphere $P_S(\beta,t\gg R^2/D_0)=\frac{1}{2}\sin\beta$, while for a cylinder it is a constant, $P_C(\beta,t\gg r^2/D_0)=1/2\pi$. For any surface this quantity can be calculated independently from the simulations,

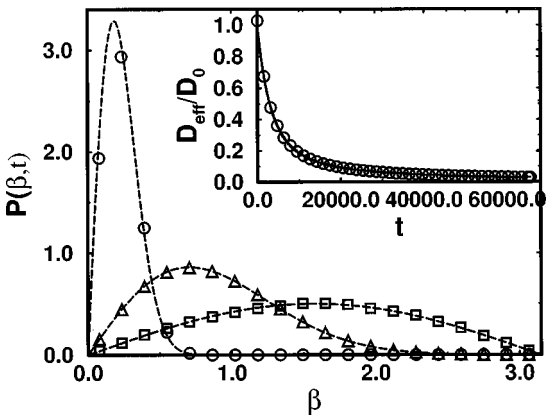

FIG. 1. The RAD $P(\beta,t)$ for a sphere of radius R as a function of the reorientational angle β (in rad) for the following diffusion times (i.e., the number of random walk steps): $t/\tau_0=64.0$ (circles), 1024.0 (triangles), and 16384.0 (squares). The inset shows the effective diffusion constant $D_{\rm eff}/D_0$, as a function of time. The solid or dashed lines represent the analytical results. In the simulations the average jump length $J=1.0\sqrt{4D_0\tau_0}$ and $R=43.0\sqrt{4D_0\tau_0}$. The typical length of one run is $T\approx 10^8\tau_0$, and the averages at time t are taken over T/t points on the trajectory.

and thus provides another way to verify the uniform stationary particle distribution on the surface (see the above discussion of the detailed balance condition). Another quantity of interest is an effective diffusion constant defined here as $D_{\rm eff}=\langle r^2(t)\rangle/4t$, where $\langle\,\rangle$ is the average over all the random walk trajectories at time t. For a sphere we have

$$D_{\rm eff}=\frac{R^2}{2t}\left[1-\exp\left(-\frac{2D_0t}{R^2}\right)\right], \tag{13}$$

and, for a cylinder,

$$D_{\rm eff}=\frac{1}{2}D_0+\frac{R^2}{2t}\left[1-\exp\left(-\frac{D_0t}{R^2}\right)\right]. \tag{14}$$

In the short time limit the effective diffusion coefficient is equal to the local diffusion coefficient (see the inset in Figs. 1 and 2). In the long time limit $D_{\rm eff}$ for a sphere goes to zero

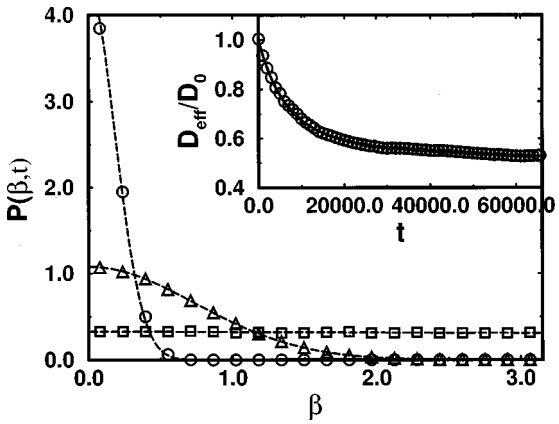

FIG. 2. The RAD $P(\beta,t)$ for a cylinder of radius R as a function of the angle β (in rad), for the following diffusion times: $t/\tau_0=64.0$ (circles), 1024.0 (triangles), and 16384.0 (squares). See also the legend of Fig. 1.

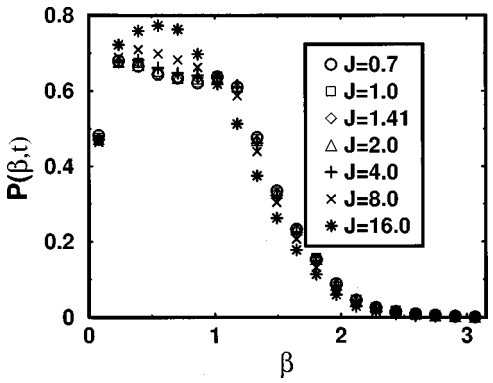

FIG. 3. The RAD $P(\beta,t)$ for a P surface the size of the unit cell $d=100.0\sqrt{4D_0\tau_0}$ for different jump lengths J [from $J=0.7\sqrt{4D_0\tau_0}$ (circles) up to $J=16.0\sqrt{4D_0\tau_0}$ (stars)] rescaled to a base time equal to $512\tau_0$ for the evolution with $J=1.0\sqrt{4D_0\tau_0}$ (squares).

due to the fact that the region available for the diffusing particle is bounded. The one for the cylinder reaches $0.5D_0$. The reduction of $D_{\rm eff}$ by a factor of 2 is obvious, because in the long time limit the particle diffuses only along one spatial dimension since the available space in the second dimension is bounded.

IV. DIFFUSION ON THE NODAL SURFACES

The convergence of the algorithm has been tested on the nontrivial P periodic nodal surface [12] given by Eq. (2) with

$$\phi(\mathbf{r})=\cos X+\cos Y+\cos Z, \tag{15}$$

where $X=2\pi x/d$, $Y=2\pi y/d$, and $Z=2\pi z/d$ in terms of the average step size varying from $J=0.7\sqrt{4D_0\tau_0}$ up to $J=16.0\sqrt{4D_0\tau_0}$, with the size of the unit cell $d=100.0\sqrt{4D_0\tau_0}$. The algorithm starts to give incorrect results for a jump length $J=8.0\sqrt{4D_0\tau_0}$ (see Figs. 3 and 4). Let us compare this jump length to the typical radius of curvature of the surface. To compute curvatures we take a unit vector normal to the surface $\mathbf{n}(\mathbf{r})$ at the point $\mathbf{r}$ on the surface proportional to the gradient of the scalar field $\phi(\mathbf{r})$:

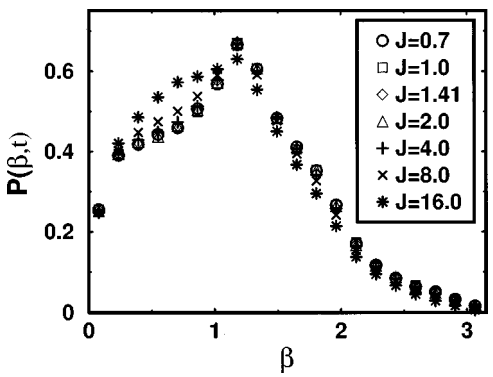

FIG. 4. The RAD $P(\beta,t)$ for a P surface the size of the unit cell $d=100.0\sqrt{4D_0\tau_0}$ for different jump lengths J [from $J=0.7\sqrt{4D_0\tau_0}$ (circles) up to $J=16.0\sqrt{4D_0\tau_0}$ (stars)] at a time equal to $1024\tau_0$ for the evolution with the jump length $J=1.0\sqrt{4D_0\tau_0}$ (squares).

$$\mathbf{n}(\mathbf{r}) = \frac{\nabla \phi(\mathbf{r})}{|\nabla \phi(\mathbf{r})|}. \tag{16}$$

The mean $(H(\mathbf{r}))$ curvature is given by the divergence of the unit vector, normal to the surface at the point $\mathbf{r}$, $\mathbf{n}(\mathbf{r})$:

$$H(\mathbf{r}) = \frac{1}{2}\left(\frac{1}{R_1} + \frac{1}{R_2}\right) = -\frac{1}{2}\nabla \cdot \mathbf{n}(\mathbf{r}), \tag{17}$$

and the Gaussian curvature $K(\mathbf{r})$ by the formula [14–16]

$$K(\mathbf{r}) = \frac{1}{R_1 R_2} = \frac{1}{2}[-(\partial_i n_j)^2 + (\nabla \cdot \mathbf{n}(\mathbf{r}))^2], \tag{18}$$

where R_1 and R_2 are two principal radii of the curvature at point $\mathbf{r}$. In the numerical calculations we use the formulas [14]

$$H = -\frac{1}{2\sqrt{\phi_x^2 + \phi_y^2 + \phi_z^2}}\frac{B}{A}, \tag{19}$$

$$K = \frac{1}{\phi_x^2 + \phi_y^2 + \phi_z^2}\frac{C}{A}, \tag{20}$$

where A, B, and C are given by

$$A = -(\phi_x^2 + \phi_y^2 + \phi_z^2), \tag{21}$$

$$B = \phi_x^2(\phi_{yy} + \phi_{zz}) + \phi_y^2(\phi_{xx} + \phi_{zz}) + \phi_z^2(\phi_{xx} + \phi_{yy}) - 2\phi_x\phi_y\phi_{xy} - 2\phi_x\phi_z\phi_{xz} - 2\phi_y\phi_z\phi_{yz}, \tag{22}$$

$$C = \phi_x^2(\phi_{yz}^2 - \phi_{yy}\phi_{zz}) + \phi_y^2(\phi_{xz}^2 - \phi_{xx}\phi_{zz}) + \phi_z^2(\phi_{xy}^2 - \phi_{xx}\phi_{yy}) + 2\phi_x\phi_z(\phi_{xz}\phi_{yy} - \phi_{xy}\phi_{yz}) + 2\phi_x\phi_y(\phi_{xy}\phi_{zz} - \phi_{xz}\phi_{yz}) + 2\phi_y\phi_z(\phi_{yz}\phi_{xx} - \phi_{xy}\phi_{xz}), \tag{23}$$

where the indices x, y, and z denote the respective derivatives. The minimal local curvature of these structures is equal to $0.15d$, i.e., $15.0\sqrt{4D_0\tau_0}$ (see Fig. 5), so the algorithm breaks down when the jump length J is comparable to the local radius of the curvature. The histogram of the mean curvature H for the P nodal surface is shown in Fig. 6.

We have also applied the algorithm to study the diffusion on the D periodic nodal surface [12] given by Eq. (2) and

$$\phi(\mathbf{r}) = \cos X \cos Y \cos Z - \sin X \sin Y \sin Z, \tag{24}$$

and a G periodic nodal surface [12] given by Eq. (2) and

$$\phi(\mathbf{r}) = \sin X \cos Z + \sin Y \cos X + \sin Z \cos Y. \tag{25}$$

The surface area in a unit cell for the P nodal surface is $2.353d^2$, the one for the D nodal surface is $3.839d^2$, and the one for the G nodal surface is $3.092d^2$. In order to compare the time evolution for these surfaces we have rescaled the size of unit cells in order to have the same area in a unit cell for each surface. The RAD's, together with the unit cells of the corresponding nodal periodic surfaces, are shown in Figs. 7–9. In the stationary limit the nodal surfaces have slightly different RAD's, although all the P, D, and G minimal surfaces (zero mean curvature at any point of the surface) have the same distributions of the vectors normal to the surfaces [17]. Next we see that the time evolution is different for different surfaces. We do not expect that this evolution would be the same for the P, D, and G minimal surfaces.

The stationary distribution is reached roughly after a time T_s proportional to the surface area of the periodic surface inside a unit cell of length d, $T_s = \beta d^{\alpha}$, with $\alpha = 2.0$ within statistical error (see Fig. 10). The P, D, and G structures are symmetric, so the stationary distribution is reached when the sum of left bins of the RAD (from 0.0 to $\pi/2$) is equal to the sum over the right bins (from $\pi/2$ to π). The long-time ef-

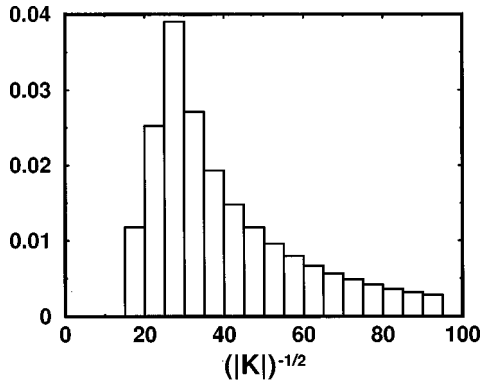

FIG. 5. The distribution of $1/\sqrt{|K|}$, where K is the Gaussian curvature for the P nodal surface. The minimal value of $1/\sqrt{|K|}$ is equal to $0.159\,52d = 15.952\sqrt{4D_0\tau_0}$, and the maximum histogram bin corresponds to $[1/\sqrt{|K|}]_m = 0.26d = 26.0\sqrt{4D_0\tau_0}$, which is the typical principal radii of curvature of the surface.

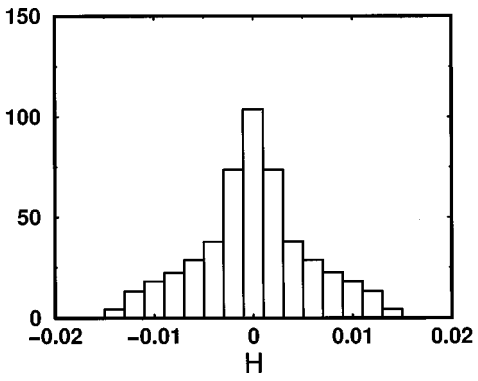

FIG. 6. The histogram for the mean curvature H of the P nodal surface.

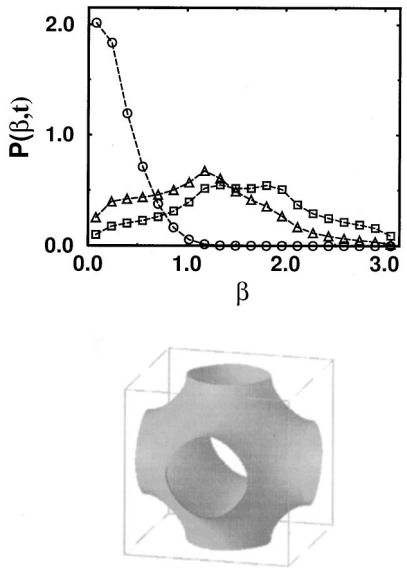

FIG. 7. The RAD for the P nodal surface for $t=64.0\tau_0$ (circles), $1024.0\tau_0$ (triangles), and $4096.0\tau_0$ (squares). The size of the unit cell (bottom) $d=100.0\sqrt{4D_0\tau_0}$ has been chosen to ensure that the P, D, and G surfaces occupy the same surface area in the unit cell (see also the legend of Fig. 1).

fective diffusion coefficient D_{eff} is equal to $(0.99\pm0.01)D_0$ (D_0 is the local diffusion coefficient). This is not surprising since in the case of the P, D, and G minimal surfaces we have the exact relation $D_{\text{eff}}=D_0$ [18], which is the upper limit for the effective diffusion coefficient on any surface. Since the P, D, and G nodal surfaces closely resemble the P, D, and G minimal surfaces (i.e., the mean curvatures of these nodal structures at any point are close to 0.0—see Fig. 6), our result has been expected.

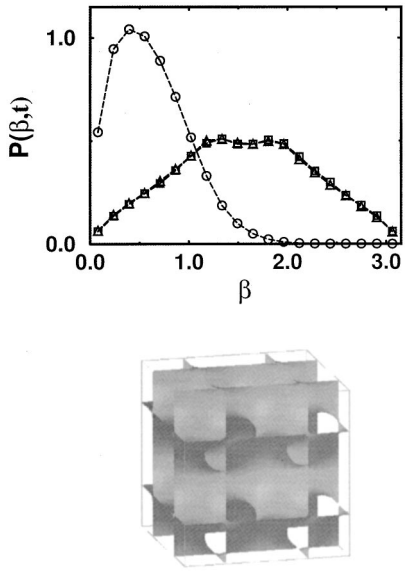

FIG. 8. The RAD (top) for the D nodal surface for $t=64.0$ (circles), 1024.0 (triangles), and 4096.0 (squares). The size of the unit cell (bottom) is $d=78.3\sqrt{4D_0\tau_0}$. Please note that for this structure the evolution is the fastest in comparison with the sphere and the P and G surfaces (see also the legend of Figs. 1 and 7).

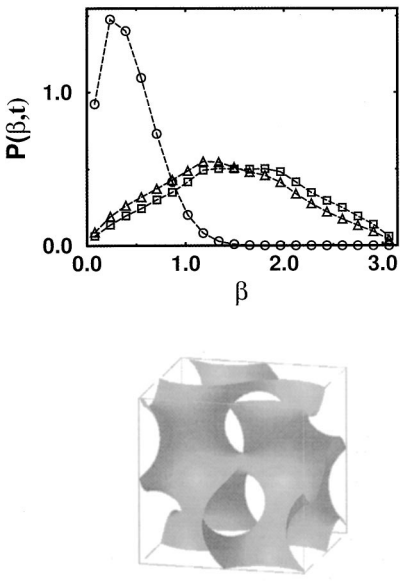

FIG. 9. The RAD (top) for the G nodal surface for $t=64.0\tau_0$ (circles), $1024.0\tau_0$ (triangles), and $4096.0\tau_0$ (squares). The size of the unit cell (bottom) is $d=87.2\sqrt{4D_0\tau_0}$ (see also the legend of Figs. 1 and 7).

V. SUMMARY

The application of our algorithm to a torus, a spherocylinder (i.e., a finite cylinder closed by spherical caps of the same radius as the cylinder), and a cylindrical surface combined with flat surfaces and minimal surfaces will allow us to study in detail the influence of the mean and Gaussian curvatures on the RAD. Since diffusion is ubiquitous, our method should find applications in various fields of physics and chemistry and not only in the particular fields mentioned here. The algorithm is very simple, and can be very efficiently used by the experimentalists for the interpretation of the NMR spectra based on the RAD distribution. Although

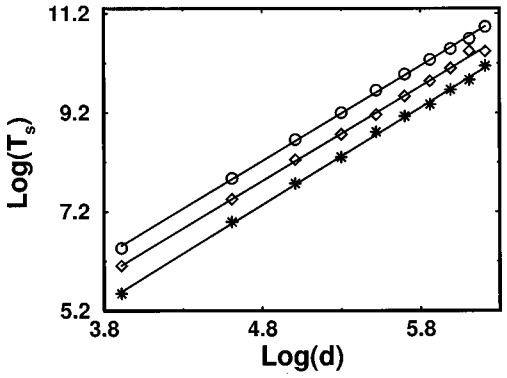

FIG. 10. The time of reaching the stationary distribution T_s vs the size of the unit cell d for the P (circles), D (diamonds), and G surfaces (stars). The stationary state is reached when the sum of left bins (from 0.0 to $\pi/2$) is equal to the sum over right bins (from $\pi/2$ to π) within chosen numerical cutoff of 5%. We find $T_s=\beta d^{\alpha}$, with α equal to 1.9 ± 0.1 (P structure), 1.9 ± 0.2 (G structure), and 2.0 ± 0.2 (D structure). The length of the unit cell d is varying from $75.0\sqrt{4D_0\tau_0}$ up to $550.0\sqrt{4D_0\tau_0}$. The β coefficient is equal to 0.26 (P), 0.17 (G), and 0.10 (D).

the formal representation of the diffusion equation on any Riemanian manifold [19,20] or on a distorted lattice [21,22] is known, to our knowledge the method for solving them in the case given by Eq. (2) has been presented only in this paper. In fact the construction of the diffusion equation on a Riemanian manifold [19] starts from the same assumption as in our algorithm, namely, that a local frame has a Euclidean structure where the diffusion can be described by an ordinary Langevin equation with a white noise or a simple random walk as in our paper. Finally, we note that a number of different methods has been developed in mathematics [23,24] in order to study isotropic transport processes on Riemanian manifolds, but so far these methods have not diffused to the physics domain.

ACKNOWLEDGMENTS

This work was supported in part by the Maria Sklodowska-Curie Joint Fund II, KBN under Grant No. 2P03B12516, and NSF Grant No. DMS-9700721.

[1] K. M. Berland, P. T. C. So, and E. Gratton, Biophys. J. **68**, 694 (1995).
[2] R. Swaminathan, C. P. Hoang, and A. S. Verkman, Biophys. J. **72**, 1900 (1997).
[3] H. Ogawa, S. Inouye, F. I. Tsuji, K. Yasuda, and K. Umesono, Proc. Natl. Acad. Sci. USA **92**, 11 899 (1995).
[4] M. P. Sheetz, S. Turney, H. Qian, and E. L. Elson, Nature (London) **340**, 284 (1989); G. M. Lee, A. Ishihara, and K. A. Jacobson, Proc. Natl. Acad. Sci. USA **88**, 6274 (1991).
[5] P. P. Mitra, P. N. Sen, L. M. Schwartz, and P. Le Doussal, Phys. Rev. Lett. **68**, 3555 (1992).
[6] M. Kac, Am. Math. Monthly **73**, 1 (1966).
[7] S. Wefing and H. W. Spiess, J. Chem. Phys. **89**, 1219 (1988).
[8] F. Macquaire and M. Bloom, Phys. Rev. E **51**, 4735 (1995).
[9] C. Dolainsky, M. Unger, M. Bloom, and T. Bayerl, Phys. Rev. E **51**, 4743 (1995).
[10] C. Dolainsky, P. Karakatsanis, and T. M. Bayerl, Phys. Rev. E **55**, 4512 (1997).
[11] A. A. Nevzorov, T. P. Trouard, and M. F. Brown, Phys. Rev. E **55**, 3276 (1997).
[12] A. L. Mackay, Proc. R. Soc. London, Ser. A **442**, 47 (1993).
[13] T. Landh, FEBS Lett. **369**, 13 (1995).
[14] I. S. Barnes, S. T. Hyde, and B. W. Ninham, J. Phys. Colloq. **51**, C7-19 (1990).
[15] A. L. Mackay and J. Klinowski, Comput. Math. Appl. **12B**, 803 (1986).
[16] M. Spivak, *A Comprehensive Introduction to Differential Geometry* (Publish or Perish, Berkeley, 1979), Vol. III.
[17] W. Góźdź and R. Hołyst, J. Chem. Phys. **106**, 9305 (1997).
[18] D. M. Anderson and H. Wennerström, J. Phys. Chem. **94**, 8683 (1990).
[19] N. Ikeda and S. Watanabe, *Stochastic Differential Equations and Diffusion Processes* (North-Holland, Amsterdam, 1981), Chap. V.
[20] R. Bausch, R. Schmitz, and L. A. Turski, Phys. Rev. Lett. **73**, 2382 (1994); Z. Phys. B **97**, 171 (1995).
[21] S. Krukowski and Ł. A. Turski, Phys. Lett. A **175**, 349 (1993).
[22] R. Bausch, R. Schmitz, and L. A. Turski, Phys. Rev. Lett. **80**, 2257 (1998).
[23] M. Pinsky, Trans. AMSE **218**, 353 (1976).
[24] Y. Amit, Stoch. Proc. Appl. **37**, 213 (1991).